Inorganic Chemistry

pubs.acs.org/IC Article

Microwave Spectra and Theoretical Calculations for Two Structural Isomers of Methylmanganese Pentacarbonyl

Chakree Tanjaroon, Zunwu Zhou, David Mills, Kristen Keck, and Stephen G. Kukolich*

Cite This: *Inorg. Chem.* 2020, 59, 6432−6438 Read Online

ACCESS | Metrics & More | Article Recommendations

ABSTRACT: The first microwave rotational spectra for two structural isomers of methylmanganese pentacarbonyl were measured in the 4−9 GHz range using a pulsed-beam Fourier transform microwave spectrometer. The spectra for the two isomers, a symmetric-top structure and an asymmetric-top acyl isomeric structure, were fit to obtain rotational and centrifugal distortion constants and ^{55}Mn quadrupole coupling parameters. The rotational constants, the manganese (^{55}Mn) nuclear quadrupole coupling constant, the centrifugal distortion constants, and the spin−rotation constant were determined for the symmetric $CH_3Mn(CO)_5$ and have the following values: $A = B = 793.153(3)$ MHz, $D_J = 0.00040(4)$ MHz, $D_{JK} = 0.0018(2)$ MHz, $C_{cc} = 0.183(6)$ MHz, and $eQq_{cc} = -87.4(3)$ MHz. Rotational constants and ^{55}Mn quadruple coupling constants were determined for the isomeric acyl-$CH_3C(O)Mn(CO)_4$ and have the following values: $A = 839.96(4)$ MHz, $B = 774.20(7)$ MHz, $C = 625.63(1)$ MHz, and $1.5\ eQq_{aa} = 44.9(47)$ MHz and $0.25(eQq_{bb} - eQq_{cc}) = 11.9(12)$ MHz. The measured rotational constants from the isomeric acyl-$CH_3C(O)Mn(CO)_4$ were compared with various theoretical computations. The calculated rotational constants for the dihapto-acyl and the agostic-acyl structures are reasonably close to the experimental values. We note that the calculated dihapto-acyl structure most closely matches the experimental data, as the calculation for the dihapto structure using the B3LYP functional with the aug-cc-pVDZ basis set closely reproduced the experimental values for *A*, *B*, and *C*.

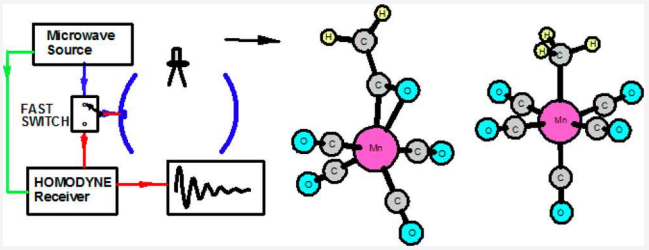

1. INTRODUCTION

The methyl manganese pentacarbonyl complex and the reaction intermediates involved in thermal carbonylation and photodecarbonylation reactions have been studied extensively. Kinetic experiments[1,2] and infrared spectroscopy studies[3] have revealed and confirmed the existence of relatively stable acyl-Mn isomers involved in the methyl migration or carbonyl insertion mechanisms (isomerization). Calderazzo and Cotton[1] were first to note that the acyl-Mn isomer $CH_3C(O)Mn(CO)_4$ must exist in rapid equilibrium with $CH_3Mn(CO)_5$ based on the observed reaction rate and the *cis*-$CH_3C(O)Mn(CO)_4$ byproduct of Calderazzo.[3] Extensive quantum chemical calculations of free and solvated structural isomers of methylmanganese pentacarbonyl have confirmed that the stable $CH_3Mn(CO)_5$ undergoes structural rearrangement during thermal cabonylation to form the acyl-Mn isomer, as does photodecarbonylation of the acylmanganese pentacarbonyl $CH_3C(O)Mn(CO)_4$.[4] This important reaction step is shown in eq 1 below.

$$CH_3Mn(CO)_5 \rightarrow CH_3C(O)Mn(CO)_4 \quad (1)$$

The free energy difference between the reactant and product in eq 1 is estimated using density functional theory to be between 8−10 kcal/mol.[5−7] Two distinct isomers of acyl-Mn isomers have been predicted to be relatively stable on the reaction potential energy surfaces. Figure 1 shows the chemical structures for the lowest energy isomer and the two distinct acyl-Mn isomers: the agostic and dihapto forms.

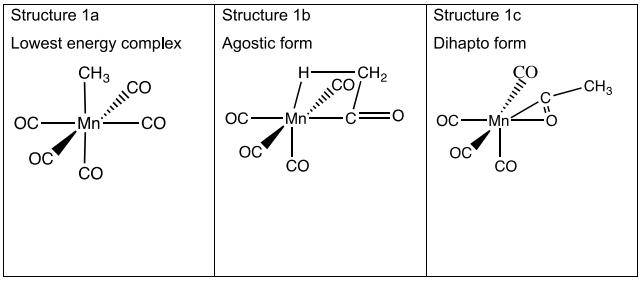

Figure 1. Three structural isomers of methyl manganese pentacarbonyl complex. Structure 1a is the lowest energy structural isomer.

Received: February 19, 2020
Published: April 22, 2020

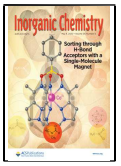

https://dx.doi.org/10.1021/acs.inorgchem.0c00524
Inorg. Chem. 2020, 59, 6432−6438

Structural data for these two different asymmetric top acyl isomeric conformations could provide valuable information on the acyl intermediates involved in migratory insertion reactions. The overall scheme of the migratory insertion reaction for methylmanganese pentacarbonyl is shown in Figure 2, in which the nucleophile CO reacts with $CH_3Mn(CO)_5$ to generate the acyl complex $CH_3C(O)Mn(CO)_5$.

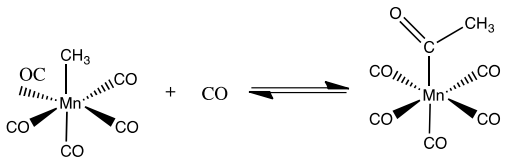

Figure 2. Scheme for CO migratory insertion reaction for $CH_3Mn(CO)_5$.

The migratory insertion reaction illustrated in Figure 2 is especially intriguing because it has two potential pathways. The first pathway is considered migratory (Figure 3), where the nucleophilic methyl ligand acts as σ donors to the carbonyl C atom cis to it, leaving one coordination site for the additional carbonyl ligand to come in.

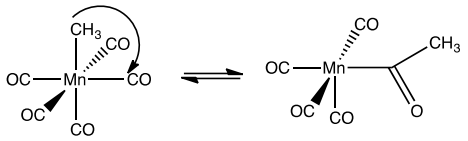

Figure 3. Scheme for migratory insertion reaction for $CH_3Mn(CO)_5$ via CH_3 migration.

The second pathway for the migratory insertion reaction in $CH_3Mn(CO)_5$ is described as an insertion (Figure 4), where

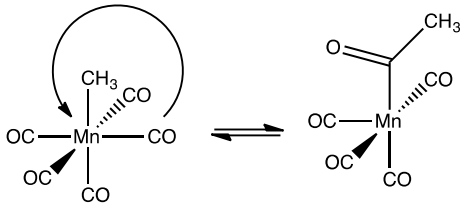

Figure 4. Scheme for migratory insertion reaction for $CH_3Mn(CO)_5$ via CO insertion.

the carbonyl ligand cis to the methyl ligand would "inject" itself between the methyl carbon and central metal, leaving one coordination site for the additional carbonyl ligand to come in.

This microwave spectroscopic study can help to support the preference for either or both of the asymmetric top isomeric acyl-$CH_3C(O)Mn(CO)_4$ conformations based on the experimental results.

Other nucleophiles that participate in migratory insertion reactions that follow similar schemes include phosphines and amines. Migratory insertion reactions in general are fundamental to organometallic chemistry and the mechanism of bond forming between carbon atoms, as shown in Figure 2, and can provide insight into industrial applications especially in catalytic carbonylation reactions.[8,9] Carbonylation reactions such as alkene hydroformylation and methanolic synthesis of acetic acid[10] are the key to the mass industrial production of alkene and acetic acid, so the understanding of migratory insertion reactions is essential. As shown in Figure 2, CO migratory insertion reactions take place between the Mn central metal atom and methyl group, and information such as the rotational barrier of a methyl group and Mn−C bond lengths can reveal much about how the alkyl group affects the migratory reaction and its dynamics.[11] The comprehension of the migratory insertion reaction can also help us extend applications into the biological field. For instance, the manganese-α-amino acid derivative was studied and synthesized through the sequential insertion of CO and imines into a manganese−carbon bond.[12]

Thermal carbonylation and photodecarbonylation reactions were carried out in organic solvents.[1,2] In this case, the solvent molecules can play a significant role in stabilizing the reaction intermediates and influence the overall structural properties and reaction rate. As far as we know, the free acyl-Mn isomers (structures 1b and 1c in Figure 1) have never been experimentally observed in the gas phase.

The gas-phase structure of $CH_3Mn(CO)_5$, the lowest energy structural isomer (1a), has been previously studied with jet-cooled infrared spectroscopy techniques.[13] The jet-cooled infrared spectrum revealed that this isomer is a symmetric top molecule with a B rotational constant of 0.0265 cm^{-1} (794. MHz) and high methyl internal rotation energy barriers. The acyl-Mn isomers, on the other hand, are expected to display asymmetric top spectra. While the presence of manganese nuclear quadrupole hyperfine can complicate the analysis of high-resolution spectra, the observation and analysis of hyperfine transitions help us in the assignment of the manganese-containing spectral carriers and reduce the chances for possible incorrect assignments due to contaminants. Previously, we have shown that distinct structural isomers of transition metal complexes as well as weakly bound complexes can be captured in the jet-cooled beam using our heated pulsed nozzle system with neon as a carrier gas.[14−16]

In this work, we have combined the resolving power of the Fourier transform pulsed-beam microwave technique with high-level quantum chemical calculations to characterize the structures of methyl manganese pentacarbonyl complexes and the associated structural isomers involved in its thermal carbonylation and photodecarbonylation reactions. We have obtained and analyzed the rotational spectra with a ^{55}Mn nuclear quadrupole hyperfine structure for the lowest energy isomer (structure 1a in Figure 1) and one of the acyl isomers (structures 1b or 1c in Figure 1). An analysis of the rotational constants and the manganese nuclear quadrupole hyperfine coupling constants for these isomers has yielded insight into the structural properties of these complexes unhindered by the presence of solvent molecules. The structural data for the symmetric top complex (structure 1a in Figure 5) obtained from this work are consistent with the structures determined from the jet-cooled vibrational spectra[11] and electron diffraction measurements.[17] A comparison between the theoretical and experimental rotational constants strongly suggests that the solvent-free structure of the acyl-Mn isomer is the dihapto form.

2. EXPERIMENTAL SECTION

2.1. Synthesis. $CH_3Mn(CO)_5$ was synthesized in our lab at University of Arizona using synthetic methods documented by King[18] and Edgell[19,20] with minor modifications. First, 2 g of $Mn_2(CO)_{10}$ was weighed and dissolved in 90 mL of tetraglyme in the nitrogen atmosphere drybox, as the starting material is air sensitive. The

https://dx.doi.org/10.1021/acs.inorgchem.0c00524
Inorg. Chem. 2020, 59, 6432−6438

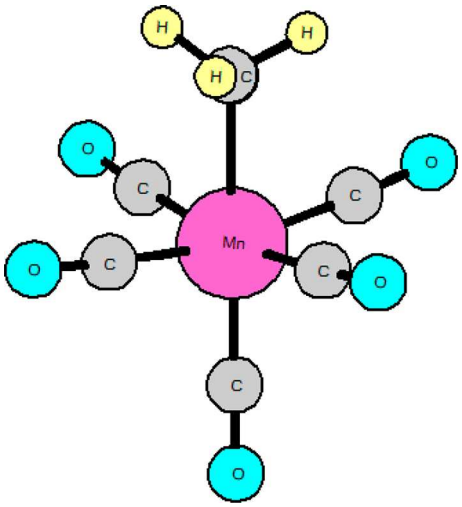

Figure 5. Symmetric top structure of the methylmanganese pentacarbonyl complex.

solution was then taken outside of the drybox, and 0.30 mL of $NaK_{2.8}$ was carefully added dropwise into the reaction flask through a syringe. $NaMn(CO)_5$ and $KMn(CO)_5$ were generated after 15 h of reaction under constant nitrogen flow and stirring. Then, 1.5 mL of methyl iodide was added into the mixture through a syringe and was allowed to react for 1 h. The final product $CH_3Mn(CO)_5$ (white solid) was precipitated during this process. Due to methylmanganese pentacarbonyl's volatile nature, the final product was vaporized and condensed into a cold trap cooled by liquid nitrogen under ~5 Torr of pressure. The white air-stable product was used without further purification and then transferred into a glass cell for rotational spectroscopic measurements.

2.2. Microwave Measurements. To facilitate the frequency search for rotational transitions of symmetric top $CH_3Mn(CO)_5$, two preferred geometries were used to generate predicted rotational spectra using the SPCAT program contained in the Pickett program suite.[21] The first geometry is the electron diffraction geometry,[17] while the second geometry is a hybrid geometry where the $Mn(CO)_5$ unit was taken from the neutron diffraction values of $HMn(CO)_5$,[22] and the CH_3−Mn bond length from the electron diffraction geometry was used. For the frequency search of asymmetric top isomeric acyl-$CH_3C(O)Mn(CO)_4$, density functional theory (DFT), partial retention of diatomic differential overlap (PRDDO),[23] and *ab initio*[24] structures were used to generate predicted spectra.

Microwave measurements were made on the vapor from $CH_3Mn(CO)_5$ in the 4−9 GHz range using a Flygare−Balle type pulsed-beam Fourier transform microwave spectrometer described previously at University of Arizona.[25,26] The glass cell containing the $CH_3Mn(CO)_5$ sample was attached to the pulse valve of the microwave spectrometer, and the sample was carried into the spectrometer by a flow of neon gas at 0.6−0.7 atm of pressure. The cell was cooled in an ice bath to reduce the vapor pressure of $CH_3Mn(CO)_5$ for optimum signals and to conserve the sample. The molecules were pulsed into the chamber of the spectrometer through a General Valve series 9 pulsed valve at 2 Hz.

2.3. Computations. The molecular structure, rotational constants, dipole moments, and quadrupole coupling strengths were calculated for symmetric, agostic, and dihapto forms of $CH_3Mn(CO)_5$ using *ab initio* and density functional calculations. Some of the starting structures were built using Spartan Version 6.1.9 and were processed with the "minimization" feature in the program. The Cartesian coordinates for each atom within the molecule were obtained after running the constructed structure under the calculation feature in the Spartan program using "Equilibrium Geometry" with B3LYP 6-31G*. The coordinates obtained were entered into input files, and the optimized structures and the harmonic vibrational frequencies were computed using the Gaussian 09 program suite.[27] Calculations were performed on the high-performance computing system (HPC) at University of Arizona. The keyword "output = pickett" was used to yield important microwave parameters such as rotational constants *A*, *B*, and *C* for comparison with experimentally determined values. MP2/Aug-cc-pVDZ, B3LYP/aug-cc-pVDZ, and M11/aug-cc-pVTZ computations were performed for the symmetric, agostic, and dihapto geometries of $CH_3Mn(CO)_5$. Frequency calculations were used to verify that the optimized geometries are a true stationary point.

The computational results for the symmetric form are displayed in Table 1, while the results for the two asymmetric, acyl isomers are displayed in Table 2.

The predicted structure and rotational constants for the symmetric form of $CH_3Mn(CO)_5$ show an oblate symmetric top ($A = B > C$). The predicted dipole moments for the DFT calculations (lines 2 and 3, Table 1) are quite small (0.007 and 0.38 D, respectively) along the *c*-axis. We note that the $A = B = B_0$ values from the first three calculations are in excellent agreement with the experimental value. The calculated rotational constants from Marynick et al.[4] are included on line 4 of Table 1. It was surprising that the values of the rotational constants from the MP2 method (last line) are much different from those by other computational methods. And the dipole moment from the MP2 method is much larger (2.9 D) than those obtained by others. The transitions were somewhat weak, and this favors the weaker dipole moments. None of the calculated quadrupole coupling values are close the measured value.

Many more calculations were done for the agostic-acyl and dihapto-acyl asymmetric isomers, and the results are shown in Table 2. The results of the computations for the agostic isomer yielded strong dipole moments along the *a*-axis and *c*-axis, with dipoles around 1.7 and 2.8 D, respectively. For the dihapto isomer, there are also strong dipole moments along the *a*-axis and *c*-axis; however, the directionality is different for the B3LYP and M11 computations. The values for the quadrupole parameters, 1.5 eQq_{aa} and $0.25(eQq_{bb} - eQq_{cc})$, vary drastically between the isomers and methods, both in sign and in magnitude. Therefore, these values were necessarily determined experimentally. The M11 calculations indicate that the dihapto form (C4) is 0.013 hartree lower in energy than the agostic form (C6). The triple-ζ B3LYP calculations indicate that the dihapto form (C3) is 0.036 hartree higher than the agostic form (C5). These calculated differences in the energies between the dihapto and agostic forms with different methods are small, inconsistent, and probably below the reliability of the present calculations. The present calculations show nearly equal energies for the dihapto and agostic forms. The very good agreements of the rotational constants for lines 2 and 4 of Table 2 favor the dihapto form. It may still be possible to observe the agostic form in other experiments. For the Marynick et

Table 1. Experimental and Calculated Rotational Constants (*A*, *B*, *C*) and *c*-Dipole Moments (D) for the Symmetric-Top Form of $CH_3Mn(CO)_5$

method/basis set	*A* (MHz)	*B* (MHz)	*C* (MHz)	μ_c (D)	eQq_{cc}	energy (Hartree)
experimental	793.153(3)	793.153(3)			−87.4(3)	
B3LYP/aug-cc-pVDZ (zz)	787.90	787.50	682.92	0.007	−355.43	−1757.758
M11/aug-cc-pVTZ (dm)	797.60	797.39	691.54	0.38	−18.55	−1757.527
Marynick[4]	798.91	798.83	694.53			
MP2/aug-cc-pVDZ (zz)	854.52	853.87	718.48	2.90	−270.37	−1755.231

https://dx.doi.org/10.1021/acs.inorgchem.0c00524
Inorg. Chem. 2020, 59, 6432−6438

Table 2. Results from the Experiments and Calculations for Asymmetric Acyl Isomeric Structures of $CH_3Mn(CO)_5$[a]

structure−method basis	A	B	C	μ_a (D)	μ_c (D)	1.5 eQq_{aa}	0.25(eQq_{bb} − eQq_{cc})	E (hartree)
experiment fit (zz)	839.96(4)	774.20(7)	625.63(1)			44.9(47)	11.9(12)	
C1 dihap B3LYP/augDZ (zz)	820.02	769.15	635.28	2.7	0.6	−73.6	1.4	−1757.752
C2 agos MP2/DZ (zz)	855.34	852.53	719.34	1.7	2.4	31.3	8.3	−1755.231
C3 DiHapto B3LYP/augTZ-DM	825.82	770.63	635.46	2.7	0.6	−55.5	−65.6	−1757.913
C4 DiHapto M11/augTZ-DM	831.15	778.28	637.94	2.1	0.9	−41.1	−84.2	−1757.575
C5 Agostic B3LYP/augTZ-DM	819.93	788.17	655.31	1.0	2.9	−88.9	−14.1	−1757.949
C6 Agostic M11/augTZ-DM	826.44	798.30	660.85	1.7	2.8	−88.9	−14.8	−1757.562
C7 Agostic B3P86 (Marynick et al.[4])	827.70	800.11	664.27					−1759.36
C8 Dihapto (Marynick et al.[4])	829.45	781.24	647.05					−1759.38

[a]Rotational constants and quadrupole coupling components are in units of MHz.

Table 3. Measured Rotational Frequencies for Symmetric Top $CH_3Mn(CO)_5$[a]

J″	K″	2F″	J′	K′	2F′	observed	σ	ν_{o-c}	N
3	2	9	4	2	11	6341.760	0.0064	0.000	7
3	1	7	4	1	9	6343.581	0.0054	0.001	4
3	1	9	4	1	11	6344.979	0.0072	0.003	5
3	0	11	4	0	13	6345.330	0.0036	0.001	5
4	2	9	5	2	11	7929.188	0.0008	−0.004	3
4	2	11	5	2	13	7929.954	0.0438	0.001	4
4	1	9	5	1	11	7930.558	0.0040	−0.004	14
4	0	9	5	0	11	7931.019	0.0053	0.001	5
4	0	13	5	0	15	7931.323	0.0036	−0.009	28
4	2	13	5	2	15	7932.603	0.0052	−0.005	4
4	3	13	5	3	15	7934.196	0.0050	−0.002	19
5	2	15	6	2	17	9518.113	0.0050	0.008	6

[a]The measurement error is σ. N denotes the number of times the frequency was measured above and below the peak. ν_{o-c} is the deviation between the measured (observed) and best fit calculated values. The values are given in MHz. The structure is shown in Figure 5.

al.[4] calculations (last two lines (C7 and C8), Table 2), both the rotational constants and energies favor the dihapto form, but agreement with the experimental values is only fair.

3. RESULTS OF MEASUREMENTS

3.1. Symmetric $CH_3Mn(CO)_5$. The symmetric top isomer has five main rotational transitions falling within the frequency range of the spectrometer. Two of these transitions, $J = 6 \rightarrow 7$ and $J = 2 \rightarrow 3$, lie near the cutoff frequencies of the spectrometer where the microwave power is low. We did not observe these two transitions in this measurement during the extensive frequency scan. The transitions for $J = 4 \rightarrow 5$ and $J = 3 \rightarrow 4$ show the characteristic ^{55}Mn nuclear quadrupole hyperfine splittings that are consistent with the predicted hyperfine spectra. For the $J = 5 \rightarrow 6$ transitions, only one $\Delta F = +1$ hyperfine transition was observed. In total, 12 rotational transitions, including some hyperfine splittings from the ^{55}Mn quadruple coupling, were observed based on the predictions for the symmetric structure and are listed in Table 3. N denotes the number of times the line was measured, and the transition with the larger N value indicates a stronger transition. Twelve hyperfine components from the three main transitions were enough to allow for the proper determination of the rotational and nuclear quadrupole coupling constants from the splitting pattern. Having the transitions from $J = 6 \rightarrow 7$ and $J = 2 \rightarrow 3$ would have allowed for a better least-squares fit analysis of these molecular constants. The measured transitions were given quantum assignments using the SPFIT program in the Pickett program suite in order to fit the important rotational parameters. These five variable parameters include the rotational constant B, the estimated manganese nuclear quadrupole coupling constant eQq_{cc}, the centrifugal distortion constants D_J and D_{JK}, and the spin−rotation constant C_{cc} (See Table 3). Quantum numbers J, K, and F in Table 1 were used in the assignments to represent the different angular momenta. J corresponds to the rotational angular momentum. K is the projection of J onto the $Mn-CH_3$ symmetry axis. F is the total angular momentum resulting from the coupling between J and ^{55}Mn nuclear spin, where $F = J + I$. The molecular parameters obtained from the fit are listed in Table 4.

Table 4. Molecular Parameters Obtained for Symmetric Top $CH_3Mn(CO)_5$ from a Least-Squares Fit to the Measured Transitional Frequencies Listed in Table 3[a]

parameters	$CH_3Mn(CO)_5$	σ
B	793.1529	0.0026
D_J	0.00040	0.00004
D_{JK}	0.0018	0.0002
C_{cc}	0.183	0.006
eQq_{cc}	−87.38	0.34

[a]The standard deviation is σ. The eQq_{cc} and C values are for ^{55}Mn. The values are given in MHz.

3.2. Asymmetric Acyl Isomeric $CH_3Mn(CO)_5$. For the asymmetric top isomeric acyl-$CH_3C(O)Mn(CO)_4$, the 4−8 GHz frequency range was scanned for rotational transitions using the same experimental conditions as those for symmetric top $CH_3Mn(CO)_5$. The acyl asymmetric top structures of the methylmanganese pentacarbonyl complex are shown in Figure 6. The asymmetric top acyl isomeric $CH_3Mn(CO)_5$ was

https://dx.doi.org/10.1021/acs.inorgchem.0c00524
Inorg. Chem. 2020, 59, 6432−6438

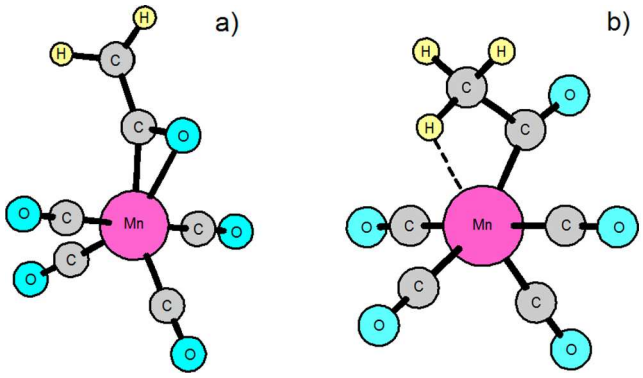

Figure 6. Acyl asymmetric top structures of the methylmanganese pentacarbonyl complex, (a) dihapto and (b) agostic, with the labeling scheme of the atoms indicated.

expected to have many *a*-dipole and *c*-dipole transitions due to asymmetry splitting, quadrupole coupling, and potential internal rotation of the methyl group. Overall, more than 100 transitions were observed during the frequency scan for asymmetric top acyl isomeric $CH_3Mn(CO)_5$, all of which fall into $J = 2$ to $J' = 3$, $J = 3$ to $J' = 4$, $J = 4$ to $J' = 5$, and $J = 5$ to $J' = 6$ categories and are listed in Table 5. The hyperfine splittings were well resolved, and the transitions were fit to within 10−20 kHz, especially in $J = 3$ to $J = 4$ transitions. In addition to the hyperfine splittings, further splittings of a few kHz were also observed, which could result from internal rotation of the methyl group. In addition, 31 transitions out of over 100 transitions were used to fit five variable parameters through the SPFIT program in the Pickett suite program. The fitted parameters, *A*, *B*, *C*, 1.5 eQq_{aa}, and $0.25(eQq_{bb} - eQq_{cc})$ are given in Table 6. The remaining measured lines, however, could not be assigned to this asymmetric top acyl isomeric model. The spectral origin of these extra lines is not known at this time. The additional lines could be from the agostic structure, or the spectrum could be contaminated with impurities in the sample and transitions from unknown molecular complexes or fragments. The five fitted parameters include the rotational constants *A*, *B*, and *C* and the quadrupole coupling constants for ^{55}Mn 1.5 eQq_{aa} and

Table 6. Fitted Structural Parameters for the Isomeric Acyl-$CH_3C(O)Mn(CO)_4$ from Experimental Data[a]

parameters	isomeric acyl-$CH_3C(O)Mn(CO)_4$
A	839.955(42)
B	774.203(67)
C	625.628(14)
1.5 eQq_{aa}	44.9(47)
$0.25(eQq_{bb} - eQq_{cc})$	11.9(12)

[a]The standard deviation for the fit is 39 kHz.

Table 5. Measured Rotational Transitions and the Deviations (ν_{o-c}) from the Calculated Values for the Isomeric Acyl-$CH_3C(O)Mn(CO)_4$

J''	K_a''	K_c''	F'' + 1/2	J'	K_a'	K_c'	F' + 1/2	observed	ν_{o-c}
3	3	1	4	2	2	1	3	4948.9594	−0.0453
3	3	1	5	2	2	1	4	4950.4983	0.0045
3	3	1	4	2	2	1	4	4950.5316	0.0375
4	1	3	2	3	1	2	2	5569.8458	−0.0079
4	1	3	2	3	1	2	1	5570.2344	−0.0114
4	1	3	3	3	1	2	4	5570.5930	−0.0094
4	1	3	3	3	1	2	3	5571.0200	0.0191
4	1	3	7	3	1	2	6	5571.0740	−0.0168
4	1	3	3	3	1	2	2	5571.4692	−0.0330
4	3	1	4	3	2	1	4	6370.9890	−0.0283
4	1	3	4	3	0	3	3	6412.0250	0.0199
4	1	3	7	3	0	3	6	6414.4418	0.0062
5	0	5	5	4	0	4	5	6432.3209	0.0230
4	2	3	3	3	1	3	2	6433.2608	−0.0188
5	0	5	5	4	0	4	6	6433.4830	0.0151
5	1	5	8	4	1	4	7	6434.0269	0.0086
4	2	3	6	3	1	3	6	6434.3279	0.0203
5	1	5	7	4	1	4	6	6434.4547	0.0113
5	1	5	3	4	1	4	2	6434.6960	0.0093
5	0	5	3	4	0	4	2	6435.0490	−0.0152
5	1	5	6	4	1	4	5	6435.2163	−0.0039
5	0	5	6	4	0	4	5	6435.5720	−0.0221
4	4	1	2	3	3	1	1	6615.7941	0.0226
4	4	1	6	3	3	1	5	6615.9956	0.0242
4	4	1	4	3	3	1	4	6618.1196	−0.0272
6	1	6	8	5	1	5	7	7685.8123	−0.0062
6	0	6	8	5	0	5	7	7685.8522	−0.0149
6	1	6	4	5	1	5	3	7686.0696	0.0242
6	1	6	7	5	1	5	6	7686.3640	−0.0078
6	1	6	5	5	1	5	4	7686.7366	0.0047
6	0	6	6	5	0	5	5	7686.8336	0.0070

https://dx.doi.org/10.1021/acs.inorgchem.0c00524
Inorg. Chem. 2020, 59, 6432−6438

$0.25(eQq_{bb} - eQq_{cc})$. The assigned 31 transitions are listed in Table 5 using quantum numbers J, K_a, K_c, and F. The best fit experimental parameters are given in Table 5 along with the same parameters given by different computations.

5. DISCUSSION

Table 4 lists the important molecular parameters for the gas phase symmetric top $CH_3Mn(CO)_5$. $A = B = B_0$ is the only rotational constant determined. The value of rotational constant B_0 = 793.1529(63) MHz is in good agreement with values from both electron diffraction (B_0 = 800.2(80) MHz) and infrared spectroscopy (B_0 = 795.6(16) MHz) data. It is a good indication that the gas phase symmetric top $CH_3Mn(CO)_5$ closely resembles the structure studied with infrared spectroscopy. The present DFT calculated results are in excellent agreement with the data, with B_0 = 787.90, 797.60, and 798.9 MHz. The centrifugal distortion constant D_J has a value of 0.40 kHz, which is considered to be relatively small. This is in agreement with the assumption that symmetric top $CH_3Mn(CO)_5$ has a rigid structure. The centrifugal stretching of the Mn−CH_3 and Mn−CO bonds does not have a significant impact on the centrifugal distortion constants. The ^{55}Mn nuclear spin−rotation constant C_{cc} has a value of 183(6)kHz, which is fairly large for a symmetric top molecule with a small C value. This indicates the possible presence of a low-lying electronic excited state. The ^{55}Mn nuclear quadrupole coupling constant obtained from the least-squares fit for the symmetric isomer is −87.38(34) MHz. This value is 1.6 times smaller than that of $HMn(CO)_5$ (−144.22(2) MHz). This indicates that $CH_3Mn(CO)_5$ has a more symmetric charge distribution around the Mn nucleus compared to $HMn(CO)_5$.

From comparing the values in Table 2, two of the calculations using the B3LYP functional (C1 and C3) for the dihapto structure most closely reproduced the experimental values for rotational constants A, B, and C. The ratios of calculated to experimental values for A, B, and C for C1 are 97.6, 99.3, and 101.5%, respectively, and for C3 are 98.3, 99.5, and 101.6%, respectively. This comparison indicates that the observed asymmetric top isomeric acyl-$CH_3C(O)Mn(CO)_4$ spectrum is most likely dihapto-stabilized acyl-$CH_3Mn(CO)_5$. The calculated rotational constants for line 4 of Table 2 also support the assignment of the spectra to the dihapto isomeric acyl-$CH_3C(O)Mn(CO)_4$.

6. CONCLUSIONS

The rotational spectrum of symmetric and asymmetric top acyl isomeric methylmanganese pentacarbonyl species was obtained. Twelve rotational transitions were assigned and used to determine the rotational constant, the estimated manganese nuclear quadrupole coupling constant, the centrifugal distortion constants, and the spin−rotation constant for the symmetric $CH_3Mn(CO)_5$. Additionally, 31 rotational transitions were assigned and used to determine the rotational constants and quadruple coupling constants for the asymmetric acyl form of $CH_3Mn(CO)_5$. On the basis of comparisons for the calculated and experimental rotational constants, the agreement is better for the dihapto structure than for the agostic structure. This indicates that the gas-phase isomeric acyl-$CH_3C(O)Mn(CO)_4$ more likely adopts a dihapto-stabilized structure. We cannot entirely rule out the agostic structure because rotational constants for both structures are similar, and the present calculations are not sufficiently accurate to make a positive assignment.

AUTHOR INFORMATION

Corresponding Author

Stephen G. Kukolich − *Department of Chemistry and Biochemistry, University of Arizona, Tucson, Arizona 85721, United States*; orcid.org/0000-0002-8229-8423; Email: kukolich@email.arizona.edu

Authors

Chakree Tanjaroon − *Department of Chemistry and Biochemistry, James Madison University, Harrisonburg, Virginia 22807, United States*

Zunwu Zhou − *Department of Chemistry and Biochemistry, University of Arizona, Tucson, Arizona 85721, United States*

David Mills − *Department of Chemistry and Biochemistry, University of Arizona, Tucson, Arizona 85721, United States*

Kristen Keck − *Department of Chemistry and Biochemistry, University of Arizona, Tucson, Arizona 85721, United States*

Complete contact information is available at: https://pubs.acs.org/10.1021/acs.inorgchem.0c00524

Notes

The authors declare no competing financial interest.

ACKNOWLEDGMENTS

This material is partially based upon work supported by the National Science Foundation under Grant No. CHE-1057796 at the University of Arizona. We are grateful for the support. The authors thank Eddie White for helping us synthesizing the complex and maintaining the drybox.

REFERENCES

(1) Calderazzo, F.; Cotton, F. A. Carbon Monoxide Insertion Reactions. I. the Carbonylation of Methyl Manganese Pentacarbonyl and Decarbonylation of Acetyl Manganese Pentacarbonyl. *Inorg. Chem.* **1962**, *1*, 30−36.

(2) Noack, K.; Ruch, M.; Calderazzo, F. Carbon Monoxide Insertion Reaction. VI. The Mechanisms of the Reactions of Methylmanganese Pentacarbonyl and Acetylmanganese Pentacarbonyl with Triphenylphosphine. *Inorg. Chem.* **1968**, *7*, 345−349.

(3) Noack, K.; Calderazzo, F. Carbon Monoxide Insertion Reactions V. *J. Organomet. Chem.* **1967**, *10*, 101−104.

(4) Derecskei-Kovacs, A.; Marynick, D. S. A New Look at an Old Reaction: The Potential Energy Surface for the Thermal Carbonylation of $Mn(CO)_5CH_3$. The Role of Two Energetically Competitive Intermediates on the Photodecarbonylation of $Mn(CO)_5(COCH_3)$. *J. Am. Chem. Soc.* **2000**, *122*, 2078−2086.

(5) Wang, X.; Weitz, E. A Density Fucntional Theory Study of Alkyl Group Migration in $RMn(CO)_5$ Complexes. *J. Organomet. Chem.* **2004**, *689*, 2354−2360.

(6) Wang, X.; Weitz, E. A Density Functional Theory Study of $\eta 2$ Acyl Bonding in Fe and Mn Carbonyl Complexes. *J. Phys. Chem. A* **2002**, *106*, 11782−11790.

(7) Boese, W. T.; Ford, P. C. Intermediates Relevant to the Carbonylation of Manganese Alkyl Complexes Interrogated by Time Resolved Infrared and Optical Spectroscopy. *J. Am. Chem. Soc.* **1995**, *117*, 8381.

(8) Henrici-Olive, G.; Olive, S. *Catalyzed Hydrogenation of Carbon Monoxide*; Springer-Verlag: Berlin, Germany, 1984.

(9) Parshall, G. W.; Ittle, S. D. Hydrogenation and Other Hydrogen-Based Catalytic Reactions. In *Homogeneous Catalysis*, 2nd ed.; Wiley-Interscience: New York, 1992.

https://dx.doi.org/10.1021/acs.inorgchem.0c00524
Inorg. Chem. 2020, 59, 6432−6438

(10) Massick, S. M.; Mertens, V.; Marhenke, J.; Ford, P. C. Reactive Intermediate Relevant to the Carbonylation of $CHMn_3(CO)_5$. Activation Parameters for Key Dynamic Processes. *Inorg. Chem.* **2002**, *41* (13), 3553−3559.
(11) Andersen, J. M.; Moss, J. R. Alkylmanganese Pentacarbonyls. *J. Organomet. Chem.* **1992**, *439* (1), C25.
(12) Lafrance, D.; Davis, J. L.; Dhawan, R.; Arndtsen, B. A. Insertion of Imines and Carbon Monoxide into Manganese-Alkyl Bonds: Synthesis and Structure of a Manganese-alpha-Amino Acid Derivative. *Organometallics* **2001**, *20* (6), 1128−1136.
(13) Gang, J.; Pennington, M.; Russell, D. K.; Davies, P. B.; Hansford, G. M.; Martin, N. A. Infrared Laser Spectroscopy of Jet-cooled Methyl Manganese Pentacarbonyl. *J. Chem. Phys.* **1992**, *97*, 3885−3891.
(14) Tanjaroon, C.; Keck, K. S.; Kukolich, S. G. Microwave Spectroscopy Measurements of Rotational Spectra and DFT Calculation for Two Distinct Structural Isomer of 1,1'-Dimethylferrocene. *J. Am. Chem. Soc.* **2004**, *126*, 844−850.
(15) Tanjaroon, K.; Daly, A. M.; Kukolich, S. G. The Rotational Spectrum and Structure for the Argon-Cyclopentadienyl Thallium van der Waals Complex: Experimental and Computational Studies of Non-Covalent Bonding in an Organometallic π-Complex. *J. Chem. Phys.* **2008**, *129*, 054305.
(16) Tanjaroon, C.; Subramanian, R.; Karunatilaka, C.; Kukolich, S. G. Microwave Measurements of 14N and D Quadrupole Coupling for (Z)-2-Hydroxypyridine and 2-Pyridone Tautomers. *J. Phys. Chem. A* **2004**, *108*, 9531−9539.
(17) Seip, H. M.; Seip, R.; Søtofte, I.; Rasmussen, S. E.; Shimizu, A. On the Structure of Methylmanganese Pentacarbonyl, $CH_3Mn(CO)_5$. *Acta Chem. Scand.* **1970**, *24*, 3431.
(18) King, R. B.; Eusch, J. J. *Organometallic Synthesese*; Academic Press: New York, 1965; Vol. *1*, p 158.
(19) Edgell, W. F.; Risen, W. M. The Mass Spectrum and Preparation of Pure Manganese Pentacarbonyl Hydride. *J. Am. Chem. Soc.* **1966**, *88*, 5451.
(20) Edgell, W. F.; Lyford, J. Preparation of Sodium Cobalt Tetracarbonyl. IV. *Inorg. Chem.* **1970**, *9*, 1932.
(21) Pickett, H. M. J. The Fitting and Prediction of Vibration-Rotation Spectra with Spin Interaction. *J. Mol. Spectrosc.* **1991**, *148*, 371.
(22) La Placa, S. J.; Hamilton, W. C.; Ibers, J. A.; Davison, A. Nature of the Metal-Hydrogen Bond in Transition Metal-Hydrogen Complexes. Neutron and X-ray Diffraction Studies of Beta-Pentacarbonylmanganese Hydride. *Inorg. Chem.* **1969**, *8* (9), 1928−1935.
(23) Axe, F. U.; Marynick, D. S. *Organometallics* **1987**, *6*, 572−580.
(24) Halgren, T. A.; Lipscomb, W. N. Self-Consistent- Field Wavefunctions for Complex Molecules. The Approximation of Partial Retention of Diatomic Differential Overlap. *J. Chem. Phys.* **1973**, *58*, 1569.
(25) Bumgarner, R. E.; Kukolich, S. G. Microwave Spectra and Structure of HI-HF Complexes. *J. Chem. Phys.* **1987**, *86*, 1083.
(26) Tackett, B. S.; Karunatilaka, C.; Daly, A. M.; Kukolich, S. G. Microwave Spectra and Gas-Phase Structural Parameters of Bis(η5-Cyclopentadienyl)Tungsten Dihydride. *Organometallics* **2007**, *26*, 2070−2076.
(27) Frisch, M. J.; Trucks, G. W.; Schlegel, H. B.; Scuseria, G. E.; Robb, M. A.; Cheeseman, J. R.; Scalmani, G.; Barone, V.; Petersson, G. A.; Nakatsuji, H.; Li, X.; Caricato, M.; Marenich, A.; Bloino, J.; Janesko, B. G.; Gomperts, R.; Mennucci, B.; Hratchian, H. P.; Ortiz, J. V.; Izmaylov, A. F.; Sonnenberg, J. L.; Williams-Young, D.; Ding, F.; Lipparini, F.; Egidi, F.; Goings, J.; Peng, B.; Petrone, A.; Henderson, T.; Ranasinghe, D.; Zakrzewski, V. G.; Gao, J.; Rega, N.; Zheng, G.; Liang, W.; Hada, M.; Ehara, M.; Toyota, K.; Fukuda, R.; Hasegawa, J.; Ishida, M.; Nakajima, T.; Honda, Y.; Kitao, O.; Nakai, H.; Vreven, T.; Throssell, K.; Montgomery, J. A., Jr.; Peralta, J. E.; Ogliaro, F.; Bearpark, M.; Heyd, J. J.; Brothers, E.; Kudin, K. N.; Staroverov, V. N.; Keith, T.; Kobayashi, R.; Normand, J.; Raghavachari, K.; Rendell, A.; Burant, J. C.; Iyengar, S. S.; Tomasi, J.; Cossi, M.; Millam, J. M.; Klene, M.; Adamo, C.; Cammi, R.; Ochterski, J. W.; Martin, R. L.; Morokuma, K.; Farkas, O.; Foresman, J. B.; Fox, D. J. *Gaussian 09*, Revision A.1; Gaussian, Inc., Wallingford CT, 2016.

https://dx.doi.org/10.1021/acs.inorgchem.0c00524
Inorg. Chem. 2020, 59, 6432−6438